Machine Copy for Proofreading, Vol. x, y–z, 2014

Optimizing Startup Frequency Setting of the Inductive Power Transfer System

Zhi-Hui Wang[1, *], Jing Wu[1], Yue Sun[1], and Xiao Lv[2]

Abstract—Based on energy injection and free resonant mode, an approach to optimize the startup frequency setting of the voltage-fed inductive power transfer (IPT) system is proposed to mitigate the effects of uncertain system parameters and load conditions. Differential equations of the primary resonant network on the free resonant mode is firstly established, then the free resonant frequency with different parameters and load conditions is calculated and verified with the soft-switching frequency of system based on stroboscopic mapping modeling method and fixed points theory. By controlling the micro-energy injection of system and free resonance, the frequency of free resonant mode is detected, and is regarded as the fixed frequency of startup process. Hence, the proposed strategy solves the uncertainty of the startup frequency and system re-setting to fit with changed system parameters and load conditions. This method also initiates immediate protection when the system operates under zero loads. In sum, our experimental results verify the theoretical implication, effectiveness, and merits of the proposed approach.

1. INTRODUCTION

Inductive power transfer (IPT) refers to the use of space electromagnetic coupling to transfer electricity power from a stationary power source to one or more movable loads [1, 2]. As an innovative technology, it is known for its safeness, efficiency and flexibility, and thus it gains increasing attention in academic research and shows prospects of industrial use [3–8].

The frequency stability of the IPT system is basis of guaranteeing the power transmission and system stability. Furthermore, the IPT system usually works in variable-frequency control mode to attain the soft-switch state with the Zero Current Switch (ZCS) or the Zero Voltage Switch (ZVS), so as to reduce switching losses of the inverter network and to ensure the efficient and stable operation of the system. Nevertheless, the system often starts up with a fixed-frequency because of the unstable factors during the startup process and then changes to the variable-frequency control mode later when its operation becomes stable. To ensure a smooth transition from the fixed-frequency mode to the variable-frequency control mode, operation frequency of the two modes should remain similar. However, as operation frequency varies with power supply, system parameters and load conditions, it is often preset in the controller under the fixed-frequency control mode. Thus, the operation frequency under the variable-frequency control mode may deviate from that of the fixed-frequency mode if it fails to fit with changed operating voltages, system parameters and load conditions. This may lead to an unstable transition between the two modes, or resonance failure, and even system crash.

To tackle above issues, an approach based on energy injection and freedom resonant mode is proposed to optimize the startup frequency of the voltage-fed IPT system. This method ensures a smooth transition from the fixed-frequency startup mode to the variable-frequency control mode under uncertain supply, system parameters and load conditions. It also helps to reduce the necessity to reset the operation frequency by changing the settings under fixed-frequency control mode. Besides, it creates

Received 20 January 2014

* Corresponding author: Zhi-Hui Wang (wzhcqu@hotmail.com).

[1] Automation College, Chongqing University, China. [2] Chongqing Special Equipment and Inspection and Research Institute, China.

a safe and reliable operation environment by protecting the system immediately when it is under zero loads.

2. SYSTEM ANALYSIS AND MODELING

In the IPT system, coupling coils are used to transmit energy from the primary side to the secondary side. Figure 1 illustrates the structure of a typical IPT system. In the primary side, the 50 Hz alternating current (AC) is firstly rectified to stable direct current (DC), and then inverted to high frequency sinusoidal current, which drives the primary coupling coil to generate high frequency sinusoidal alternating magnetic field in the near space. The secondary coupling coil generates electromotive energy in this field, which then feds into power regulation circuits such as high-frequency rectifier and DC-DC regulator to provide power for electrical appliances. Compensation capacitors are used in the primary and secondary coupling coils to improve the system's power transfer capability and to reduce VA (Voltage-Ampere) rating of the power source [9].

Based on the compensation style of the primary and secondary sides, voltage-fed IPT systems can be classified into two types: SS (primary in series and secondary in series) and SP (primary in series and secondary in parallel). The present paper focuses on the SP-type IPT system with the full-bridge inverter circuit, as shown in Figure 2.

In Figure 2, the primary electromagnetic compatibility (EMC) protection and frequency rectifier filter circuit are not illustrated. The load R_L represents the power regulation circuits and electrical equipment in the secondary side. E_{dc} is the DC voltage generated from frequency rectifier and filter. C_p and C_s refer to the compensation capacitors, while L_p and L_s are resonant inductors of the primary and the secondary sides. M stands for the mutual inductance between L_p and L_s. R_p and R_s refer to equivalent series resistance of the primary and secondary inductances. I_p and I_s are the resonance current of the primary and the secondary sides. V_p refers to the high-frequency square wave voltage formed by the inverter tank.

A mathematical model of the SP-type IPT system (showed in Figure 2) is established based on AC impedance analysis. As the secondary inductor equivalent series resistance $R_s \ll \omega L_s$, R_s can be neglected, the impedance Z_r reflected from the secondary circuit to the primary circuit can be expressed as:

$$Z_r = \omega^2 M^2 / Z_s = \frac{\omega^2 M^2 R_L}{R_L^2(\omega^2 C_s L_s - 1)^2 + \omega^2 L_s^2} - j\frac{\omega^3 M^2 \left[C_s R_L^2(\omega^2 C_s L_s - 1) + L_s\right]}{R_L^2(\omega^2 C_s L_s - 1)^2 + \omega^2 L_s^2} = R_r + j\mathrm{Im}Z_r \quad (1)$$

where ω is the operating frequency of the IPT system, and Z_s is the total impedance of the secondary side. R_r and $\mathrm{Im}Z_r$ stand for the real and imaginary parts of Z_r, respectively.

When the imaginary part of impedance Z_t from the power supply equals zero, then:

$$\mathrm{Im}Z_t(\omega, R_L, M) = \omega L_p - \frac{1}{\omega C_p} - \frac{\omega^3 M^2 \left[C_s R_L^2(\omega^2 C_s L_s \text{ - } 1) + L_s\right]}{R_L^2(\omega^2 C_s L_s \text{ - } 1)^2 + \omega^2 L_s^2} = 0 \quad (2)$$

Thus, angle frequency ω of SP-type IPT system in the zero phase can be known. According to Formula (2), the operating frequency ω will change as the load conditions (R_L and mutual inductance M) change. For a given system, when $M = 0$ (no load operation, when the secondary side is

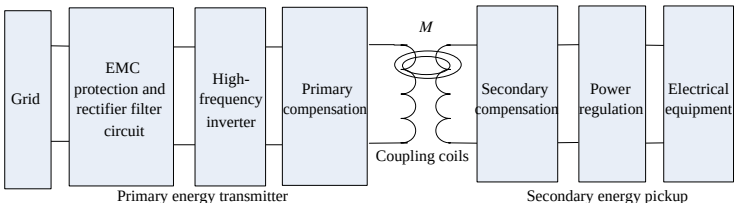

Figure 1. Structure of the IPT system.

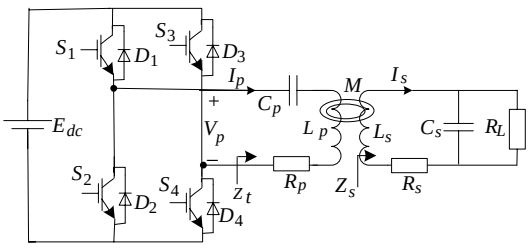

Figure 2. An SP-type IPT system with full-bridge inverter circuit.

completely decoupled from the primary side), the operating frequency of the system can be expressed as $\omega = 1/\sqrt{L_p C_p} = \omega_p$.

3. OPTIMIZATION ON STARTUP FREQUENCY BASED ON ENERGY INJECTION AND FREE RESONANT MODE

3.1. Energy Injection and Free Resonant Mode

As shown in Figure 3, during the time of $\tau_0 \sim \tau_1$, the switch pairs (S_1, S_4) and (S_2, S_3) of the primary side are turned on complementarily and energy will be quickly injected into the resonance network. At the time of τ_1, switches S_1 and S_3 are turned off, but S_2 and S_4 are on. Thus, the energy stored in L_p and C_p is alternately released by (S_2, D_4) and (S_4, D_2) and consumed by resistance R_p and the real part of Z_r. Therefore under the free resonant mode, a damped oscillation pattern is shown by the primary resonant current i_p.

3.2. Analysis of Free Resonant Mode Circuit and Verification on Soft Switching Frequency

Under the free resonant mode, as no energy is injected into the primary resonant network ($V_p = 0$), the equivalent circuit of the primary side can be shown as Figure 4 (ignoring the diode switching loss and conduction loss).

The reflected impedance Z_r may be inductive, capacitive or resistive. Assume $Z_r = R_r + j(L_r + C_r)$ and $R_x = R_p + R_r$, when the imaginary part of the reflected impedance $\mathrm{Im}Z_r > 0$, Z_r is inductive and $C_r = 0$. Nevertheless, $\mathrm{Im}Z_r < 0$, Z_r is capacitive and $L_r = 0$. In addition, when $\mathrm{Im}Z_r = 0$, Z_r is resistive. Therefore, a second-order differential equation for the primary circuit shown in Figure 4 can be expressed as:

$$\frac{d^2 u_p(t)}{dt^2} + \frac{R_x}{L_p + L_r}\frac{du_p(t)}{dt} + \frac{1}{(L_p + L_r)(C_p + C_r)} u_p(t) = 0 \tag{3}$$

As the current of inductor would not change abruptly, at the initial time $t = 0$: $i_p(0) = 1/(L_p + L_r)$, $du_p(0)/dt = 1/(L_p + L_r)(C_p + C_r)$, $u_p(0) = 0$. Thereby the voltage of the compensation capacitor can be calculated as:

$$u_p(t) = \frac{\omega_p^2}{\omega} e^{-\alpha t} \sin \omega t \tag{4}$$

where ω_p is the natural resonant frequency of primary resonant network, ω is the damped oscillation frequency (also known as the free resonance frequency), α is the damping coefficient. In addition,

$$\begin{aligned} &\alpha = R_x/2(L_p + L_r), \quad \omega_p = 1\Big/\sqrt{(L_p + L_r)(C_p + C_r)}, \\ &\omega = \sqrt{\omega_p^2 - \alpha^2} = \sqrt{1\Big/(L_p + L_r)(C_p + C_r) - (R_x/2(L_p + L_r))^2} \end{aligned} \tag{5}$$

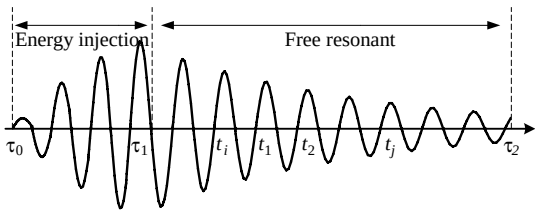

Figure 3. Energy injection and the free resonant mode.

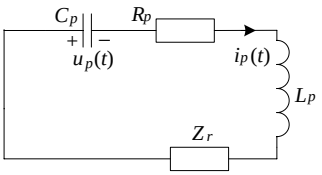

Figure 4. Equivalent circuit of the primary resonant network under the free resonant mode.

Hence, the resonant current of primary inductor i_p is derived as

$$i_p(t) = (C_p + C_r)\frac{du_p(t)}{dt} = \frac{\omega_p}{(L_p + L_r)\omega} e^{-\alpha t}\cos(\omega t + \theta) \tag{6}$$

where $\theta = \arccos(\omega/\omega_p)$, which is the phase angle difference between the current i_p and the voltage u_p.

Based on above analysis, when the system is under the free resonant mode, the peak of the primary resonant current will decay exponentially regardless of the feature of reflected impedance Z_r as shown in Formula (6). Nevertheless, the damping coefficient α, and the free resonance frequency ω will change with the load conditions (R_L and M).

As the stroboscopic mapping modeling method and fixed points theory can accurately calculate the soft-switching operating point of the resonant converter [10–12], it is used to verify whether the resonant frequency is the soft switching operating frequency under the resonant mode. Assume that the switching period of the full-bridge inverter is T under steady-state conditions shown in Figure 2, the input voltage of the resonant network can be calculated as:

$$V_p = \begin{cases} E_{\mathrm{dc}} & t \in [0, T/2) \\ -E_{\mathrm{dc}} & t \in [T/2, T) \end{cases} \tag{7}$$

Let the system state vector be $x = [u_p, i_p]^T$ and the input vector be $u = [V_p]$. Then the state-space model of the system shown in Figure 2 can be described as:

$$\dot{x} = Ax + Bu \tag{8}$$

where the coefficient matrices are:

$$A = \begin{bmatrix} 0 & \frac{1}{C_p + C_r} \\ -\frac{1}{L_p + L_r} & -\frac{R_x}{L_p + L_r} \end{bmatrix} \quad B = \begin{bmatrix} 0 \\ \frac{1}{L_p + L_r} \end{bmatrix} \tag{9}$$

So the fixed point x^* calculated based on the stroboscopic mapping modeling method and fixed points theory is shown in (10).

$$x^* = \left(I + \Phi\left(\frac{t}{2}\right)\right)^{-1}\left(I - \Phi\left(\frac{t}{2}\right)\right)A^{-1}BE_{\mathrm{dc}} \tag{10}$$

where $\Phi(t) = e^{At}$.

When the voltage-fed IPT system is under the ZCS condition as shown in Figure 2, the switches of the primary side must be switched on or switched off as soon as the current i_p turns to zero. Thus, the selection matrix should be $Y = [0,\ 1]$, and the fixed-point function to calculate the duration of the operating points under the ZCS condition is shown as:

$$i_p^*(t) = Yx^* = \frac{2(C_p + C_r)E_{\mathrm{dc}}\sinh\left(\frac{\Delta}{4(L_p+L_r)(C_p+C_r)}t\right)}{\Delta\left(\cosh\left(\frac{R}{4(L_p+L_r)}t\right) + \cosh\left(\frac{\Delta}{4(L_p+L_r)(C_p+C_r)}t\right)\right)} \tag{11}$$

where $\Delta = \sqrt{(C_p + C_r)^2 R_x^2 - 4(L_p + L_r)(C_p + C_r)}$. Based on Formulas (5) and (11), i_p can be simplified as:

$$i_p^*(t) = \frac{k\sin\left(\frac{1}{2}\omega t\right)}{\cosh\left(\frac{1}{2}\alpha t\right) + \cos\left(\frac{1}{2}\omega t\right)} \tag{12}$$

where the gain factor $k = -(C_p + C_r)E_{\mathrm{dc}}\omega_p^2/\omega$. The root value of equation $i_p^*(t) = 0$ is duration of the operating points under the ZCS condition as $T_n = 2n\pi/\omega$ ($n = 1, 2, 3, \ldots$). In addition, as the root value depends on the free resonant frequency ω, ω is thus regarded as the ZCS frequency of the system.

Therefore, the above analysis shows ω in the fixed-point function (12) corresponds to operating frequency of the system under ZCS condition. Nevertheless, as the system has multiple operating points, the system would not operate steadily in the bifurcation regions and its settings must satisfy Formula (13) [13].

$$Q_p > Q_s + 1/Q_s \tag{13}$$

where the Q_p is the quality factor of the primary side, while Q_s is that of the secondary side.

According to Formulas (1), (5) and (6), the primary resonant current is associated with the load resistance R_L and the mutual inductance M. When R_L increases, the reflected impedance Z_r, the damping coefficient α, and the free resonant frequency ω decrease, but the resonant current increases. Under the free resonant mode, when the system is on zero load (i.e., $M = 0$), the resonant current of the primary side reaches the peak value, but the resonant frequency reduces to the minimum value.

3.3. Startup Frequency Setting Method

As shown in Figure 3, the micro-energy injection happens between the time τ_0 to τ_1, the free resonant mode between $\tau_1 \sim \tau_2$, and fixed frequency startup between $\tau_2 \sim \tau_3$, τ_1 is microsecond level and τ_3 is millisecond level, so $\tau_1 \ll \tau_3$. The primary resonant current i_p is converted to an output voltage signal u_i with a small value that directly reflects the magnitude and phase of i_p through the current sensor. Then the sinusoidal signal u_i is converted to the square wave signal at the same frequency through the comparator. The controller detects the rising edge of the square wave signal to calculate the frequency of free resonant mode of the system, which will be selected as the operating frequency of fixed-frequency startup process. It indicates that when the free resonant frequency equals to the primary natural resonance frequency (i.e., $\omega = \omega_p$), the system reaches the zero load ($M = 0$) and it should automatically turns itself down as the voltage-fed IPT system cannot operate under zero load [14]. The flow chart of the startup frequency setting process is shown in Figure 5.

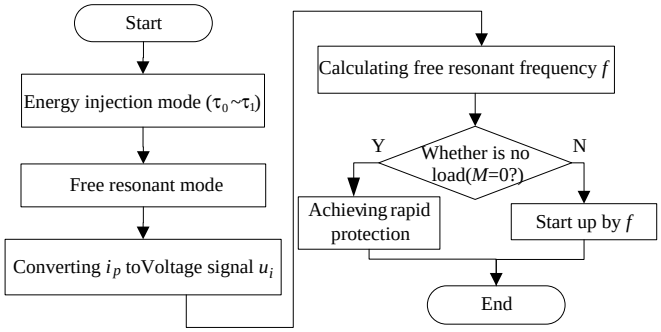

Figure 5. Flowchart of the startup frequency setting process.

Assuming that the two adjacent square wave signals reach the rising edge at the time of t_1, t_2 during the period of $\tau_1 \sim \tau_2$, then the free resonant frequency of system can be calculated as $f = 1/(t_2 - t_1)$. However, as the system is susceptible to external interference when it is in the free resonant mode, the free resonant frequency of the system needs to be computed to reduce the error by detecting the i-th rising edge time t_i and the j-th rising edge time t_j as:

$$f = (j - i)/(t_j - t_i) \tag{14}$$

Taking f calculated from Formula (14) as the startup frequency during the period of $\tau_2 \sim \tau_3$. Also this startup frequency is ZCS frequency of the system, which ensures a reliable system startup and smooth switching process from the fixed-frequency startup to the steady variable frequency operation.

4. SIMULATION AND EXPERIMENTAL RESULTS

In order to verify the theoretical analysis, a typical MATLAB/Simulink simulation model for a SP-type IPT system has been built and a corresponding experimental system have been established based on the circuit shown in Figure 2. System parameters are shown in Table 1. A CPLD chip (Altera MAX II EPM240T100C5N) is used as the controller of the IPT system. LM311 chips and IGBTs (FGA25N120) are comparator and switch devices of the full-bridge inverter circuit, respectively.

In both simulation and experimental systems, the starting time of the energy injection is $\tau_0 = 0\,\mu s$, the end time of the energy injection is $\tau_1 = 200\,\mu s$. Here the dc supply E_{dc} is assumed to be a step input of 30 V.

Table 1. Parameters of IPT simulation and experimental systems.

Parameters	Values
Primary resonant inductance L_p	152 μH
Primary resonant capacitance C_p	0.44 μF
Secondary resonant inductance L_s	364 μH
Secondary resonant capacitance C_s	0.2 μF
Equivalent series resistance R_p	0.34 Ω
Input voltage E_{dc}	30 V

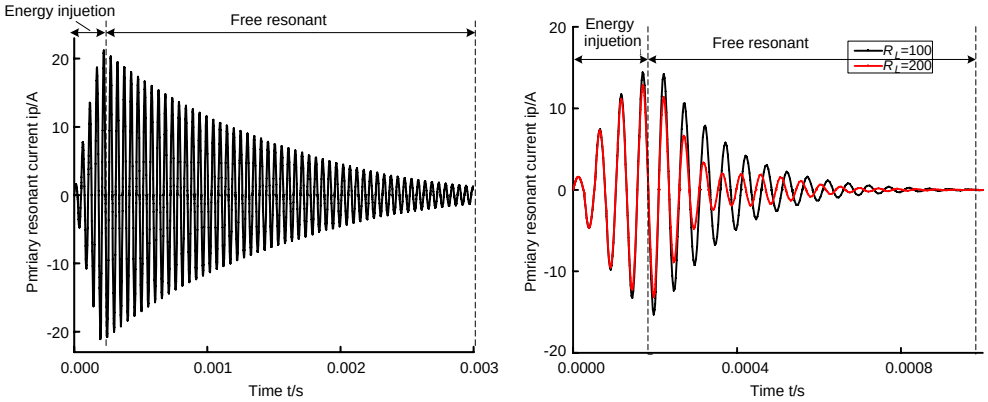

Figure 6. Simulation waveforms of the primary resonant current of the energy injection and free resonant mode. (a) No load ($M = 0$). (b) Loads of different power levels ($M = 40\,\mu\mathrm{H}$).

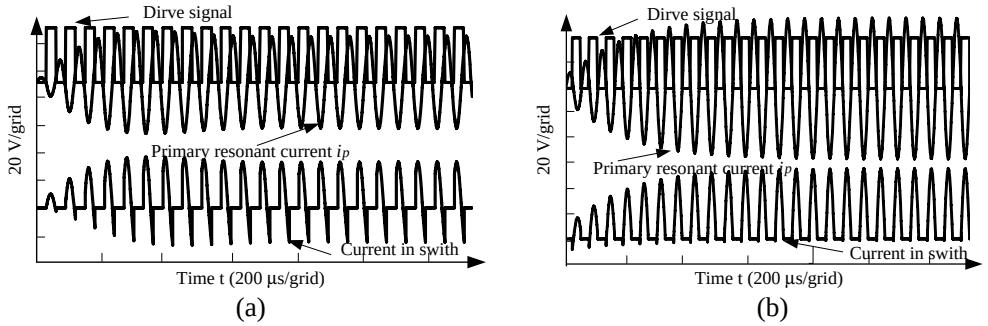

Figure 7. Simulation waveforms of fixed-frequency startup process. (a) Traditional fixed-frequency startup process. (b) Optimal fixed-frequency startup process.

Figure 6 illustrates simulation waveforms of the primary resonant current of the energy injection and free resonant mode. Figure 6(a) shows the situation under the condition of no load ($M = 0$), while Figure 6(b) shows the scenario under loads of different power levels with mutual inductance $M = 40\,\mu\mathrm{H}$. Figure 7 illustrates simulation waveforms of fixed-frequency startup process with $R_L = 100\,\Omega$, $M = 40\,\mu\mathrm{H}$. Figure 7(a) shows simulation waveforms of the traditional fixed-frequency startup process, while Figure 7(b) shows the optimal startup process of the IPT system.

The startup fixed-frequency is set to 18.66 kHz which is the natural resonance frequency of the secondary side during the energy injection period of the system. It can be calculated from Figure 6(a) that the free resonant current peak value of the primary side achieves the maximum value but the resonant frequency reaches the minimum value to 19.40 kHz in free resonant mode when the system is no load, and the error percentage between the simulation value and theoretical value ($f = 1/(2\pi\sqrt{L_pC_p})$)

19.47 kHz is 0.36%. Figure 6(b) shows that the smaller R_L (heavier load) requires the greater primary resonance current i_p and the smaller resonance frequency under the free resonant mode. It can be calculated that the free resonant frequency of the system are 20.09 kHz and 20.93 kHz with the loads of $R_L = 100\,\Omega$ and $R_L = 200\,\Omega$ respectively according to Figure 6(b). Hence, the simulation results verify the validity of the theoretical analysis that $\alpha \propto R_L$, and $\omega \propto R_L$. The startup process shown in Figures 7(a) and (b) indicate that the primary resonant current in the steady state increases 49.5% from 9.9 A RMS to 14.8 A RMS after the optimal control, which leads to the improved capability of power transfer. The phase difference between the primary resonant current and the switches driving signal results in large peaks current flowing through the switches during the traditional fixed-frequency startup process. While in the optimal fixed-frequency startup process shown in Figure 7(b), the switches are turned on or off at resonant current zero and as a result, the current flowing through S_2 is almost no peaks and ZCS startup is completely achieved.

Figure 8 shows the experimental results of energy injection and free resonant mode under different load conditions, where the startup fixed-frequency is set to 18.66 kHz. The switch pairs (S_1, S_4) and (S_2, S_3) of the primary side are turned on complementarily during the energy inject period ($\tau_0 \sim \tau_1$). Switches S_1 and S_3 are turned off, but S_2 and S_4 are on under the free resonant mode. While switches S_1 and S_4 are turned off, but S_2 and S_3 are on before τ_0 in order to ensure system security.

Figure 8 indicates that the peak value of primary resonant current i_p decreases but its frequency increases as the load decreases. The free resonant frequency are 19.35 kHz, 19.53 kHz and 20.35 kHz respectively under three conditions: no load ($M = 0$), $R_L = 100\,\Omega$ and $R_L = 200\,\Omega$. The error rates between the simulation value and experimental value are 0.26%, 2.79%, and 2.77% for the environment interferences and resistance loss in the practical circuit.

Figure 9 illustrates experimental waveforms of the traditional fixed-frequency startup process and the optimized startup process. The primary resonant current in the steady state increases 24.7% from 8.5 A RMS to 10.6 A RMS after the optimal control, showing improved capability of power transfer. Figure 9(a) shows that in the traditional fixed-frequency startup process, the value of the primary resonant current fails to reduce to zero at the moment when the switches are turned on and off, which leads to large current peaks flow through the switches and slightly distorted waveform of i_p. Therefore,

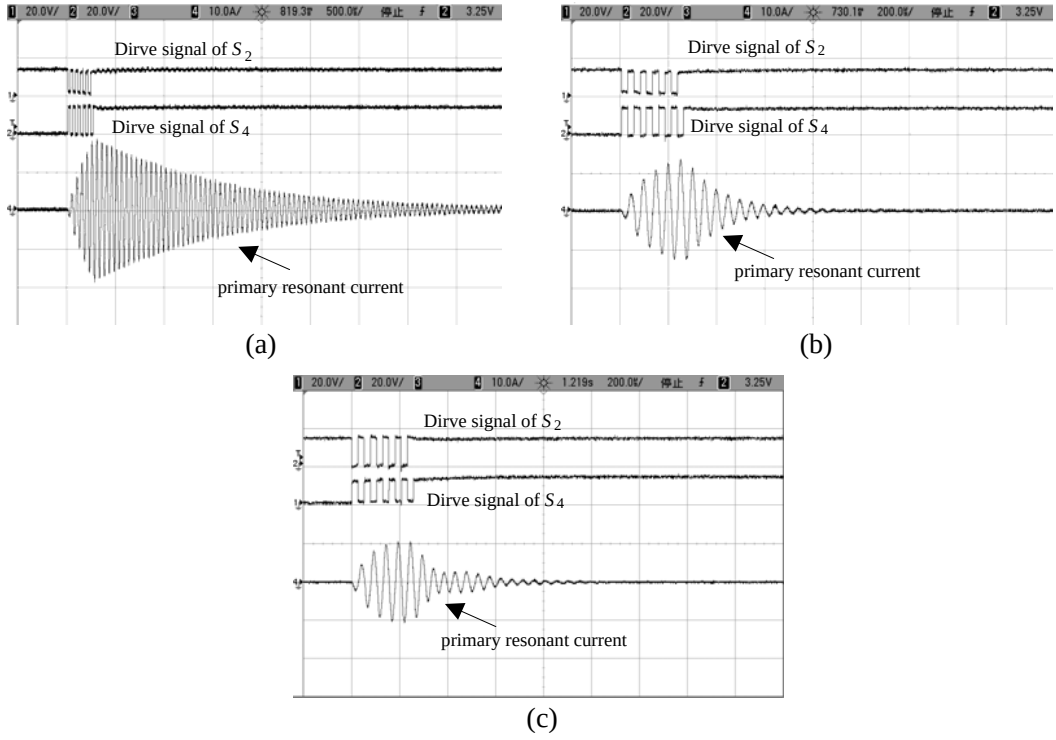

Figure 8. Experimental waveforms of energy injection and free resonant mode with different load conditions. (a) $M = 0$. (b) $R_L = 100\,\Omega$ and $M = 40\,\mu$H. (c) $R_L = 200\,\Omega$ and $M = 40\,\mu$H.

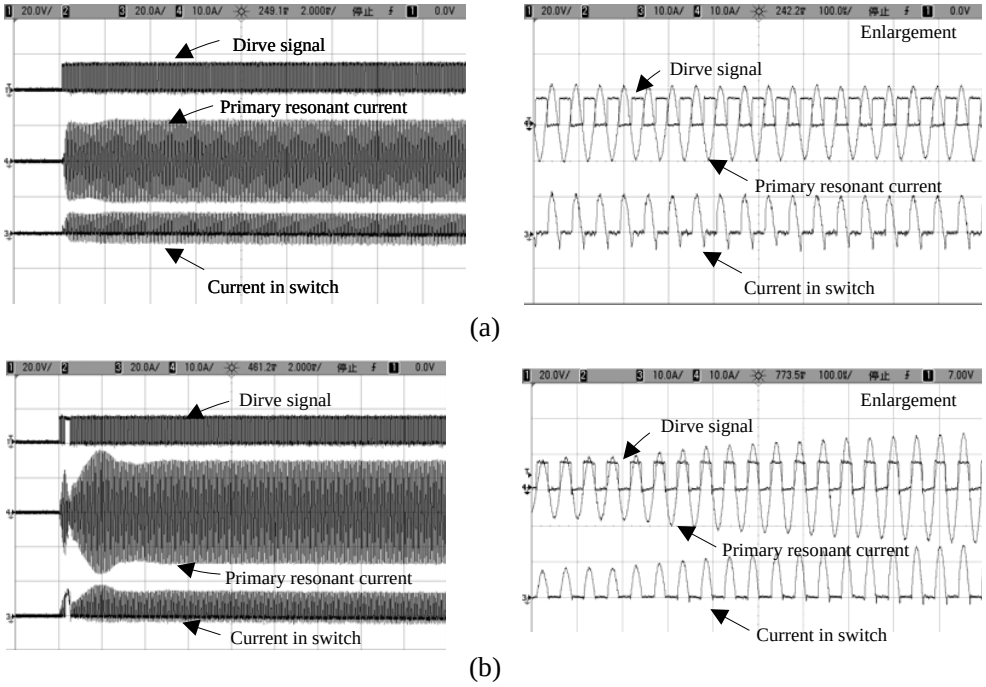

Figure 9. Experimental waveforms of fixed-frequency startup process. (a) Traditional fixed-frequency startup process. (b) Optimal fixed-frequency startup process.

the system becomes unstable and the loss will increase. By contrast, in the optimal startup process, the inverter network is switched on and off immediately. Thus, no large peak occurs in the current flowing through S_2 and ZCS operation is achieved. As a result, the system can be smoothly transited from the fixed-frequency startup to the variable-frequency control mode, which improves the stability of the system. The experimental results are also consistent with the previous theoretical analysis and simulation results.

As current-fed IPT systems cannot operate on open circuits, they work well with the proposed optimal startup strategy after changing the energy injection method.

5. CONCLUSION

This paper has proposed an optimal fixed-frequency startup method for the voltage-fed IPT system based on energy injection and free resonant mode. Injecting micro-energy instantaneously helps the system to operate with free resonance. When the system is under loads, the resonant frequency is set as the operation frequency of fixed-frequency startup. Compared with traditional fixed-frequency startup methods, the proposed method can solve the problem that startup frequency cannot be determined accurately and the setting of the system requires constant adjusting due to variation of system parameters and loads conditions. When the system is under no load, this method enables the system to be protected immediately. Besides, it also helps to reduce the system loss by achieving ZCS startup process and lowering the peak values of switches current. Thus, the system can smoothly move from the fixed-frequency startup to the variable frequency control mode, which improves the reliability, efficiency and safeness of the system. Moreover, this method can be applied not only in systems with random load changes, but also systems with unknown parameters in the startup process.

ACKNOWLEDGMENT

This research was supported by the National Natural Science Foundation of China (Nos. 51207173 & 51007100 & 51277192), the Research Fund for the Doctoral Program of Higher Education (No. 20100191120024).

REFERENCES

1. Huh, J., S. W. Lee, W. Y. Lee, G. H. Cho, and C. T. Rim, "Narrow-width inductive power transfer system for online electrical vehicles," *IEEE Trans. Power Electron.*, Vol. 26, No. 12, 3666–3679, Dec. 2011.
2. Zhong, W. X., X. Liu, and S. Y. Hui, "A novel single-layer winding array and receiver coil structure for contactless battery charging systems with free-positioning and localized charging features," *IEEE Trans. Ind. Electron.*, Vol. 58, No. 9, 4136–4144, Sep. 2011.
3. Neath, M. J., U. K. Madawala, and D. J. Thrimawithana, "A new controller for bi-directional inductive power transfer systems," *2011 IEEE Inter. Symp. Ind. Electron.*, 1951–1956, 2011.
4. Mcdonough, M., P. Shamsi, B. Fahimi, "Application of multi-port power electronic interface for contactless transfer of energy in automotive applications," *2011 IEEE Digital Object Identifier, VPPC*, 1–6, 2011.
5. Hui, S. Y. R. and W. W. C. Ho, "A new generation of universal contactless battery charging platform for portable consumer electronic equipment," *IEEE Trans. Power Electron.*, Vol. 20, No. 3, 620–627, 2005.
6. Abdolkhani, A. and A. P. Hu, "A novel detached magnetic coupling structure for contactless power transfer," *37th Annual Conference on IEEE Industrial Electronics Society, IECON 2011*, 1103–1108, 2001.
7. Matsumoto, H., Y. Neba, K. Ishizaka, et al., "Comparison of characteristics on planar contactless power transfer systems," *IEEE Trans. Power Electron.*, Vol. 27, No. 6, 2980–2993, Jun. 2012.
8. Budhia, M., J. T. Boys, G. A. Covic, et al., "Development of a single-sided flux magnetic coupler for electric vehicle IPT charging systems," *IEEE Trans. Ind. Electron.*, Vol. 60, No. 1, 318–328, 2013.
9. Zhao, Z. B., Y. Sun, Y. Zhai, and F. X. Yang, "Constant voltage output of dynamic loads in voltage-fed CPT systems," *Journal — Huazhong University of Science and Technology Nature Science Edition*, Vol. 39, No. 9, 66–70, Sep. 2011.
10. Tang, C. S., "Study on soft switching operating points of contactless power transfer system and their application," Ph.D. Dissertation, Department of Automation, Chongqing University, 2009.
11. Tang, C. S., Y. Sun, Y. G. Su, et al., "Determining multiple steady-state ZCS operating points of a switch-mode contactless power transfer system," *IEEE Trans. Power Electron.*, Vol. 24, No. 2, 416–425, 2009.
12. Tang, C. S., Y. Sun, X. Dai, et al., "Extended stroboscopic mapping (ESM) method: A soft-switching operating points determining approach of resonant inverters," *2010 IEEE International Conference on Sustainable Energy Technologies (ICSET)*, 1–5, Kandy, Sri Lanka, 2010.
13. Wang, C.-S., G. A. Covic, and O. H. Stielau, "Power transfer capability and bifurcation phenomena of loosely coupled inductive power transfer systems," *IEEE Trans. Ind. Electron.*, Vol. 51, No. 1, 148–156, Feb. 2004.
14. Wang, Z. H., "Study on contactless power transfer mode based on envelope modulation," Ph.D. Dissertation, Department of Automation, Chongqing University, 2009.